Dear Dr. Männel, Editor of ESSD

Thank you very much for considering our manuscript. We sincerely appreciate the opportunity to address the constructive comments provided by Dr. Ramillien, Hong Li, and an anonymous reviewer.

We have carefully revised our manuscript entitled "**Global satellite gravity data products for prompt detection of short-term Mass Change (MC) (essd-2025-829)**" following the comments by two reviewers. We believe we have addressed all comments and questions in the revised manuscript and this letter to the reviewers. Please see our point-by-point responses below. Reviewers' comments are highlighted in blue and our responses are shown in black.

Sincerely,

Miao Tang (lead author) and Shin-Chan Han (correspondent)
On behalf of all co-authors

Response to Reviewer #1's comments

General:

This paper joins an alternative trend in using directly range-acceleration reduced observations as a means to detect mass changes on the Earth's surface. Here, the work focuses on presenting a global time series dataset of Line-of-Sight Gravity Differences (LGDs) from (1) KBR/LRI reduced observations, (2) synthesised monthly solutions (i.e. L2), and (3) synthesised from a climatology model (i.e. climatology from monthly L2) for GRACE-FO only (2018-2024). I recommend that this paper be returned to the authors, subject to many technical corrections, which are required to make the article and dataset more reproducible.

R1C1: We sincerely thank you for your thorough review of our work. We have carefully revised the manuscript in response to these valuable comments and suggestions, particularly in terms of making the article and dataset more reproducible. Please see our point-by-point responses below. Reviewers' comments are highlighted in blue and our responses are shown in black.

Abstract:

1) Line 16: Well, if it is at satellite altitude level, it is not "in-situ". Please rephrase.

R1C2: We have removed the term "in-situ" throughout the manuscript.

2) Line 17: Be specific, which LGD dataset in particular? The monthly L2 or climatology will surely not show any sub-monthly signals.

R1C3: Here, we refer to the LGD measurements derived from the along-track KBR/LRI observations, rather than the monthly L2-LGD or the climatological LGD results. We have revised this sentence to make it clear.

3) Line 19-20: not entirely sure where 5-6 days comes from? This would mostly refer to a relatively "good" ground coverage.

R1C4: We agree that the 5–6 day interval essentially refers to a relatively "good" ground coverage. To clarify this point, we have added Figure S1, which shows the satellite ground tracks in consecutive 5-day windows during July 2020 for a low- to mid-latitude example (Figure S1a), in consecutive 5-day windows during January 2024 for comparison (Figure S1b), and in consecutive 3-day windows during July 2020 for a high-latitude example (Figure S1c). In Figures S1a and S1b, a red 4° × 4° block located in the Amazon is used to represent a typical GRACE footprint-scale area. The results show that, in low- and mid-latitude regions, the satellite ground tracks pass through such a block at least once within each 5-day period. This indicates that such regions can generally be observed at intervals of about 5–6 days. Figure S1c further confirms that the revisit interval becomes shorter toward higher latitudes due to the much denser ground-track coverage in the example region.

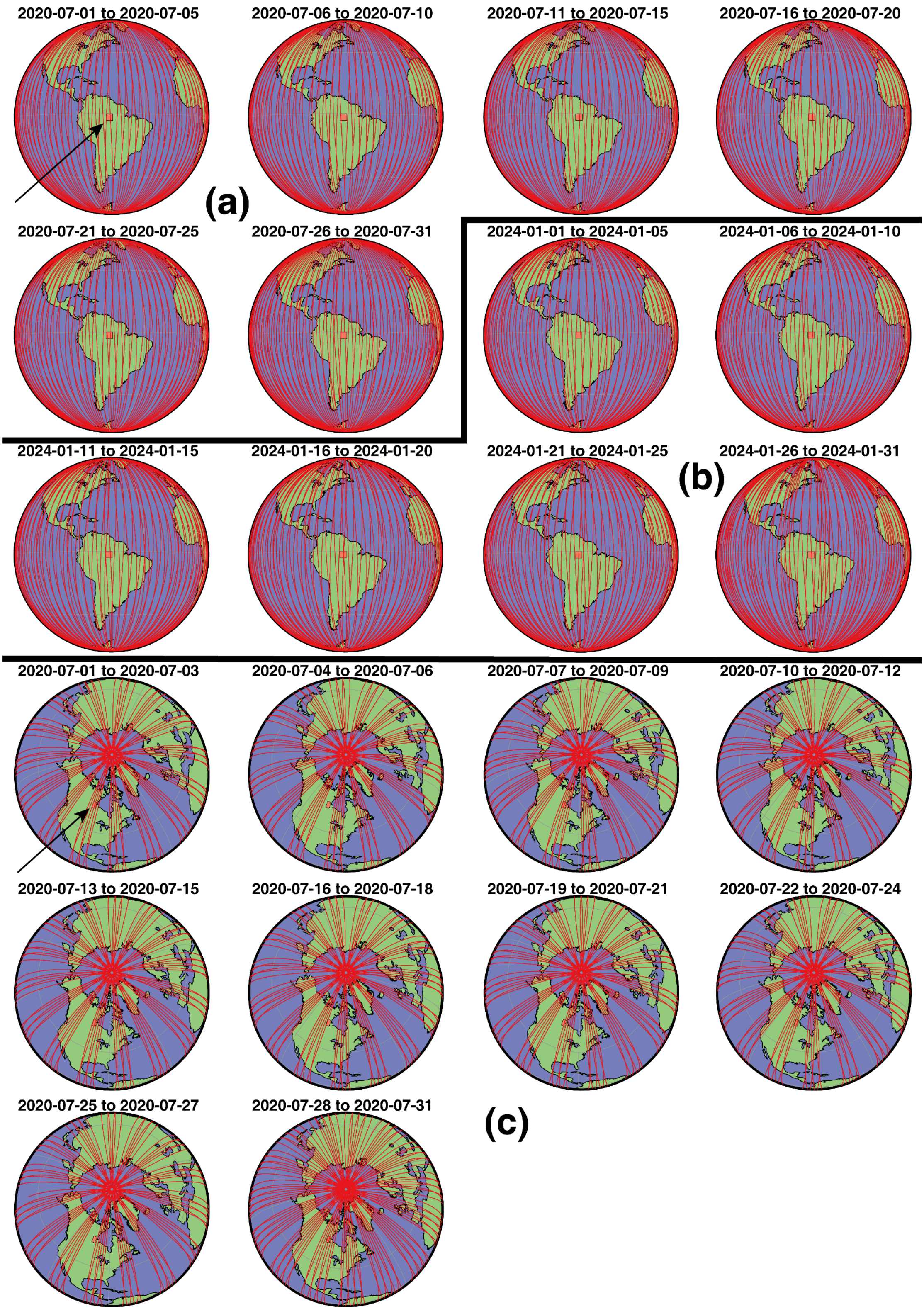

Figure S1. Satellite ground tracks (red curves) in consecutive 5-day windows during July 2020 for a low- to mid-latitude case (a), in consecutive 5-day windows during January 2024 for comparison (b), and in consecutive 3-day windows during July 2020 for a high-latitude case (c). The red 4°×4° boxes mark the study areas in the Amazon (a and b) and North America (c).

4) Line 23: Please rephrase "termination", due to the ground repeat properties of the orbit, this is not fully accurate.

R1C5: Thank you for this helpful comment. The relevant text now reads: "Results show that the LGD dataset has the potential to resolve the critical timing (e.g., onset and peak) of hydrological extremes, which is unattainable from monthly products."

Introduction:

1) Line 70: Additionally, one essential aspect of these "daily" solutions is that, effectively, their temporal resolution is not "daily" due to temporal correlation.

R1C6: Thank you for pointing this out. To reflect this aspect more accurately, we have clarified this point and added one sentence in the revised manuscript: "Note that the effective temporal resolution of these solutions is not truly daily due to the temporal correlation between adjacent epochs introduced by the Kalman smoothing framework."

2) Line 107: "minimally affected by modeling and post-processing," this is can be highly debatable. To have useful LGD datasets, you need to choose a de-aliasing product (AOD1B), an ocean tide model (there are many), a static gravity field, time filtering is also an essential aspect (how to remove low and high frequency noise?), …

R1C7: We apologize for the confusion caused by this wording. Here, by "modeling," we refer primarily to the inverse models and estimation frameworks used to generate Level-2, Level-3, or other processed GRACE products (e.g., daily solutions such as ITSG-Grace2018), which often involve complex parameterization, regularization, and solution strategies that may introduce additional uncertainty. By "post-processing," we refer primarily to the decorrelation, spatial smoothing, and scaling procedures commonly required when using Level-2 products.

We fully acknowledge that LGD processing still depends on background models and the treatment of high-frequency noise. We do not intend to suggest that LGD is free from modeling or processing assumptions. Rather, our point is that the LGD dataset is derived more directly from along-track intersatellite ranging observations, without solving a global gravity-field inversion problem or relying on the substantial post-processing typically required for monthly Level-2 or Level-3 products. In this sense, the hydrology-related instantaneous gravity variations are derived in a more observation-driven manner. High-frequency noise is treated mainly through spectral analysis and band-dependent filtering, rather than through a complex inversion framework. To address this concern, we have revised the manuscript accordingly.

3) Line 109: it does enhance temporal resolution however the spatial resolution is purely limited to the latitudinal coordinate.

R1C8: We agree that the LGD dataset does not improve spatial resolution. We have now clarified this point in the revised manuscript. In fact, our aim is to provide a dataset with high temporal resolution (but not spatial resolution) for the prompt detection of short-term mass change.

4) Line 112: again provide some rationale/explanation/source for the 5-6 days.

R1C9: Please see our response in R1C4.

Section 2:

2.1:

1) Provide some more details on how did you manage the "interpolation" between consecutive AOD1B 6/3hourly solutions.

R1C10: For a given epoch, we first identify the two neighboring AOD1B 3-hourly datasets. The Stokes coefficients are then linearly interpolated between these two epochs to obtain the coefficients at the given epoch, according to:

$$C_{nm}(t) = C_{nm}(t_0) + \frac{t - t_0}{t_1 - t_0}[C_{nm}(t_1) - C_{nm}(t_0)]$$

$$S_{nm}(t) = S_{nm}(t_0) + \frac{t - t_0}{t_1 - t_0}[S_{nm}(t_1) - S_{nm}(t_0)]$$

where t_0 and t_1 denote the two adjacent AOD1B epochs surrounding the target epoch t.

2) The same but slightly different mention of how the tidal ocean model is evaluated should be made more explicit.

R1C11: The ocean-tide-related Stokes coefficients at each epoch are evaluated directly following the formulation of the IERS Conventions (2010), using the FES2014b ocean tide model. In practice, the Delaunay variables and Greenwich Mean Sidereal Time are first computed for the given epoch, and the tidal arguments are then formed for each tidal constituent. The ocean tide coefficients are subsequently obtained by summing the harmonic contributions of all constituents:

$$\Delta C_{nm}(t) = \sum_f \left[\left(\Delta C^+_{nm,f} + \Delta C^-_{nm,f}\right)\cos\theta_f + \left(\Delta S^+_{nm,f} + \Delta S^-_{nm,f}\right)\sin\theta_f\right]$$

$$\Delta S_{nm}(t) = \sum_f \left[\left(\Delta S^+_{nm,f} - \Delta S^-_{nm,f}\right)\cos\theta_f - \left(\Delta C^+_{nm,f} - \Delta C^-_{nm,f}\right)\sin\theta_f\right]$$

Here, f denotes a tidal constituent, and θ_f is its tidal argument. The coefficients $\Delta C^+_{nm,f}$, $\Delta S^+_{nm,f}$, $\Delta C^-_{nm,f}$, $\Delta S^-_{nm,f}$ are the prograde and retrograde harmonic coefficients provided by the ocean tide model.

2.2:

1) provide the numerical differentiation algorithm for completeness and reproducibility

R1C12: The time derivative is computed using a first-order difference scheme, with forward differencing at the first epoch, backward differencing at the last epoch, and centered differencing for the interior epochs:

$$\begin{cases} y_i' = \dfrac{y_2 - y_1}{t_2 - t_1}, & i = 1 \\ y_i' = \dfrac{y_{i+1} - y_{i-1}}{t_{i+1} - t_{i-1}}, & i = 2, 3, \ldots, n-1 \\ y_i' = \dfrac{y_n - y_{n-1}}{t_n - t_{n-1}}, & i = n \end{cases}$$

Here, y_i denotes the range-rate residual at the i-th epoch. Since the orbit determination arc length is one day, the numerical differentiation is applied to the daily range-rate residual series. Accordingly, n denotes the total number of epochs within one day, which is 17,280 for KBR and 43,200 for LRI.

2) same for the temporal frequency filtering.

R1C13: We have now clarified in the revised manuscript that the temporal frequency filtering is performed using a 6th-order Butterworth band-pass filter. To avoid phase distortion, the filter is applied in a zero-phase-shift manner.

3) make explicit what part of the reference gravity field are these LGDs w.r.t. Conventionally speaking one should only remove the static part such that the full temporal gravity field signal would be conserved in your dataset.

R1C14: Thank you for pointing this out. The LGD values in our final dataset are referenced only to the static part of GOCO06s, rather than to the static, annual, and trend components combined. Although the reference orbit determination uses all three components (i.e., the static, annual, and trend parts), the LGD contributions corresponding to the annual and trend signals are added back in the final processing step. Therefore, the released LGD dataset is effectively expressed with respect to the static gravity field only, so that the full temporal gravity variations are preserved. We have clarified this point in the revised manuscript, and the corresponding processing flow is now illustrated in Figure S2:

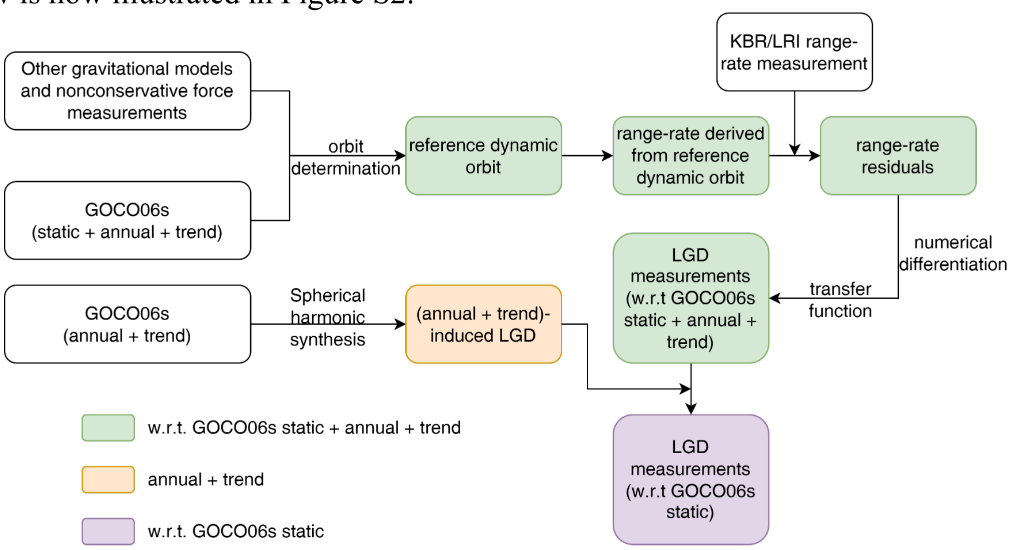

Figure S2. Processing flow for deriving the final LGD measurements with respect to the static part of GOCO06s.

4) Line 186: actually the transfer function can be used up to 0.9 mHz, with 1 mHz being a highly conservative loss of signal.

R1C15: We agree that, according to the findings in Ghobadi-Far et al. (2018), the transfer function may still be applicable down to about 0.9 mHz (~5 CPR). Our intention in adopting 1 mHz was to ensure a robust separation between the low-frequency component and the transfer-function-derived component, thereby minimizing the risk of introducing unstable signals near the lower edge of the valid band. Moreover, the signal in the 0.9–1.0 mHz waveband is not lost in our final LGD product because these low-frequency components are supplemented using the Level-2 solutions, which provide the low-frequency information below 1 mHz (approximately equivalent to SH degree lower than 6) with good accuracy.

To further clarify this point, we have carried out a test by repeating the processing with a 0.9 mHz cutoff and comparing the resulting LGD series with those obtained using the original 1 mHz cutoff. The comparison shows that the magnitudes of signal at frequencies within 0.9–1.0 mHz are quite small and do not affect the main conclusions.

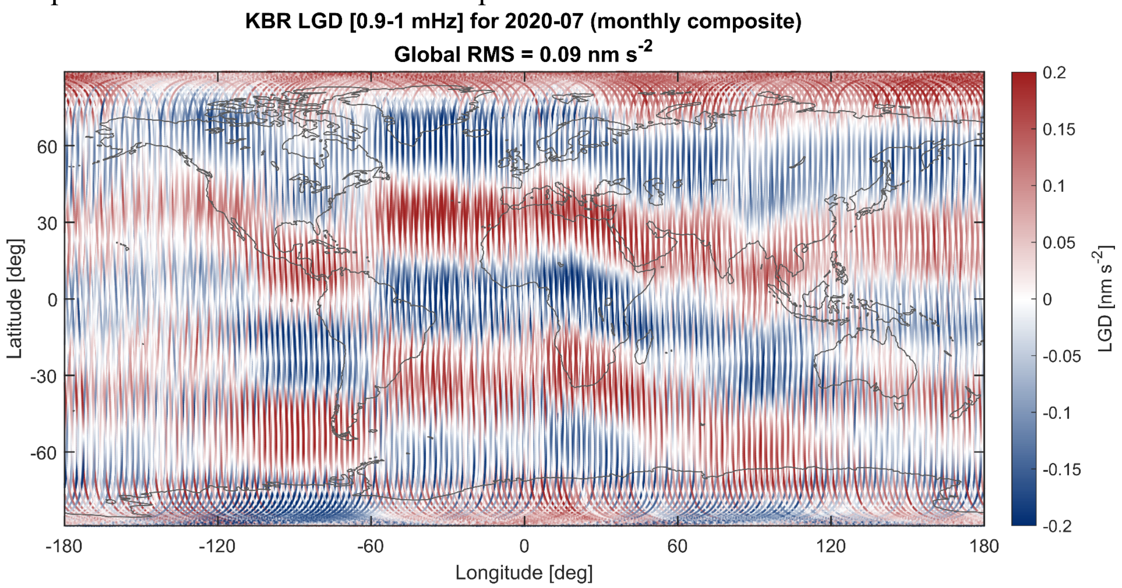

Figure S3. Global monthly composite map of KBR-LGD in the 0.9–1 mHz frequency band for July 2020.

5) Line 186-187: not very understandable which "higher frequencies" you mean. Provide more explicitly the band-pass range.

R1C16: Here, the "higher frequencies" refer specifically to frequencies higher than 1 mHz. We have revised the manuscript accordingly.

2.3:

Line 199-207:

- what is the rationale to use CSR's monthly solutions? In your case and selection of ocean tidal (and static) models, the best would be to use TU Graz's solutions. A rationale should be provided, and a check of the effect of different solutions should be conducted.

R1C17: We understand the reviewer's concerns regarding the choice of L2 products. Our purpose here is not to preserve strict background-model consistency with the orbit determination, but to provide a stable and accurate representation of the low-frequency LGD component below 1 mHz, for which CSR monthly solutions are widely used and well validated.

Following the reviewer's suggestion, we have now examined the impact of using different GRACE solutions on our results (Figure S4). Specifically, we compared the along-track LGD synthesized from four different Level-2 solutions, namely CSR (RL06.3), JPL (RL06.3), GFZ (RL06.3), and ITSG (ITSG-Grace_operational). All solutions were downloaded up to degree and order 96. After replacing $C_{2,0}$ and $C_{3,0}$, removing the GOCO06s static field, and truncating the solutions to degree and order 60, they were used to synthesize along-track LGD for 18 July 2020 (see R1C18 for the discussion of truncation processing).

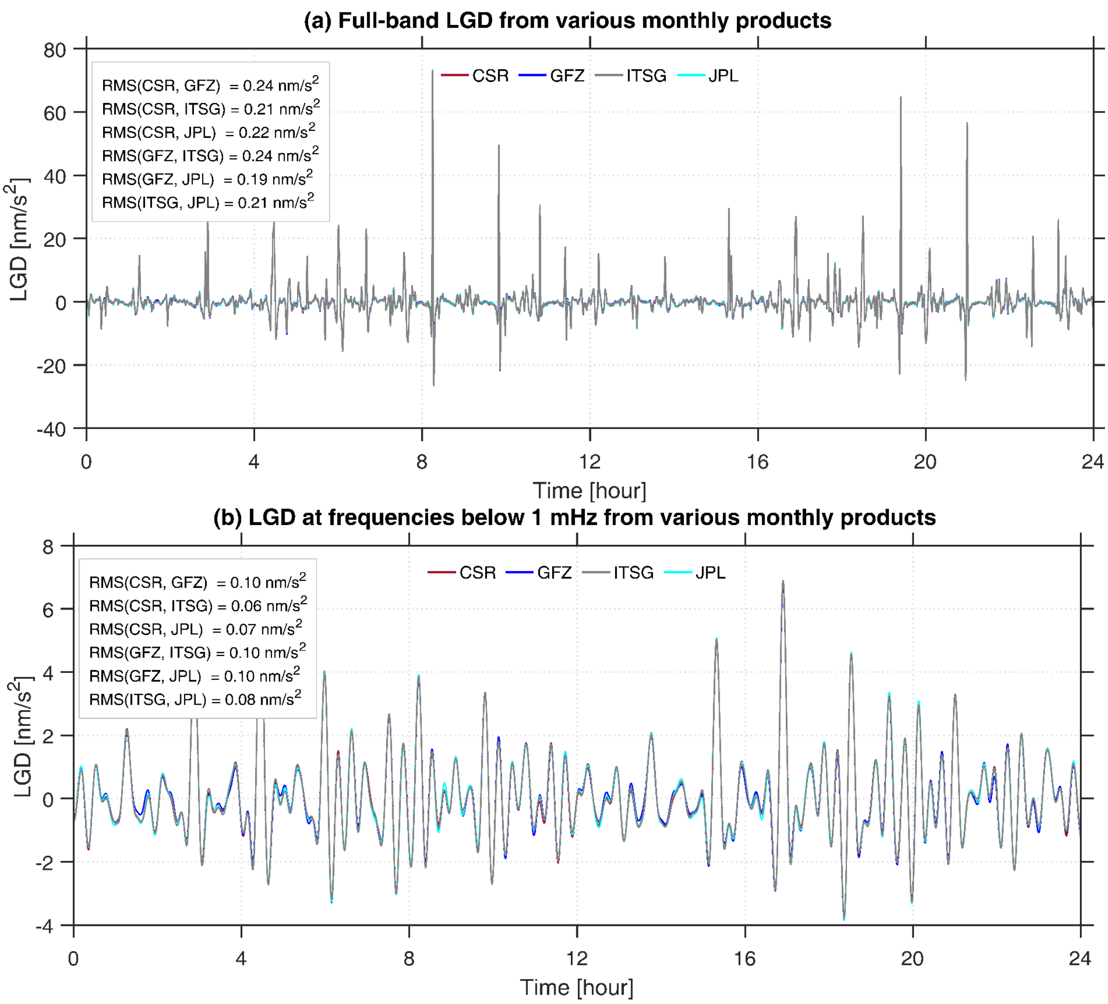

Figure S4. Along-track LGD synthesized from CSR, GFZ, ITSG, and JPL monthly solutions on 18 July 2020, compared for full-band (a) and frequencies below 1 mHz (b).

We conducted the comparison for two frequency ranges: (1) the full-band LGD (here, synthesized LGD provides frequency content up to 10 mHz), which is used to verify the LGD measurements, and (2) the low-frequency part below 1 mHz, which is used to complement the LGD measurements. For the full-band LGD (Figure S4a), the differences among the four solutions are quite small, with RMS values of only about 0.2 nm/s^2. For the low-frequency component below 1 mHz (Figure S4b), the RMSs among the four datasets are all below 0.1 nm/s^2, which is negligible for the purposes of this study.

In particular, for the low-frequency component below 1 mHz (Figure S4b), CSR shows the smallest RMS relative to the other three solutions (0.06, 0.07, and 0.10 nm/s^2), slightly lower than those of JPL (0.07, 0.08, and 0.10 nm/s^2), GFZ (0.10, 0.10, and 0.10 nm/s^2), and ITSG (0.06, 0.08, and 0.10 nm/s^2). Therefore, CSR monthly solutions show relatively good performance in the final LGD results, and the accuracy of our dataset is not sensitive to this choice.

- second, I see an issue with the truncation of a field with a max degree 96 to degree 60. You will have several issues related to truncation errors. Why not just take a field with max degree 60 in the first place? I see that this could be quite an issue.

R1C18: We agree that directly using spherical harmonic coefficients with a maximum degree of 60 is a more straightforward choice. Here, to assess whether using the degree-96 monthly products and then truncating them to degree 60 would introduce any noticeable effect, we compared LGD synthesized from three cases: (1) the native CSR degree-60 monthly products (CSR60), (2) the native CSR degree-96 monthly products (CSR96), and (3) the CSR degree-96 products truncated to degree 60 before synthesis (CSR96→60). We performed the comparison for both the full-band LGD and the low-frequency LGD below 1 mHz (same as Figure S4).

The results show that, in the frequency band below 1 mHz, the differences among the three cases are negligible (RMSs are about 0.02 nm/s^2, see Figure S5a). This indicates that, for the low-frequency component (<1 mHz), using the native degree-60 products or truncating the degree-96 products to degree 60 yields essentially the same result. Therefore, the truncation step does not affect the dataset content or any scientific conclusions based on the low-frequency LGD. This is expected because the truncated part (degrees 61 to 96) mainly corresponds to higher-frequency components and therefore does not affect the low-frequency signal below 1 mHz.

For the full-band LGD, the native degree-96 solution shows somewhat larger differences because it contains additional contributions from degrees 61 to 96 (especially from the polar region, Figure S5b). As a result, the RMS differences between the native degree-96 solution and the other two degree-60-based solutions are both about 0.35 nm/s^2. In contrast, the RMS difference between the truncated degree-96-to-60 solution and the native degree-60 solution is only 0.10 nm/s^2. Such a small difference is negligible and does not affect the LGD_L2 included in our dataset.

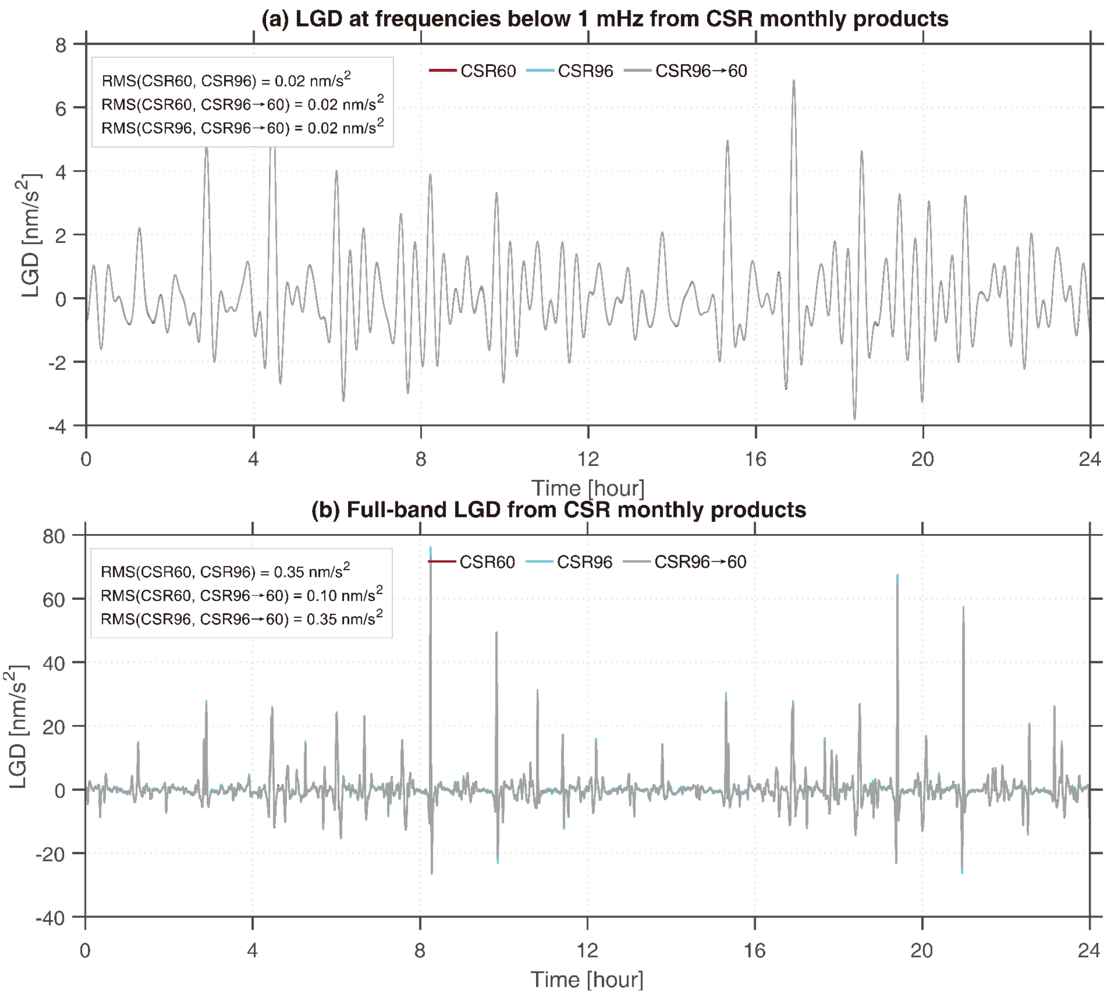

Figure S5. Along-track LGD synthesized from CSR60, CSR96, and CSR96→60 solutions on 18 July 2020, compared for frequencies below 10 mHz (a) and below 1 mHz (b).

- provide the Release of the CSR solutions + citation for reproducibility.

R1C19: We used CSR RL06.3 for GRACE-FO (https://doi.org/10.5067/GFL20-MC063) and CSR RL06 for GRACE (https://doi.org/10.5067/GFL20-MC060). We have added this information to the manuscript.

- what is the difference between KBR/LRI residuals and L2 below frequencies of 1 mHz? Why is this replacement even made, please provide some form of rationale for this.

R1C20: The line-of-sight gravity difference can be expressed as (see Equation (2) in Ghobadi-Far et al. (2018)):

$$g_{12}^{LOS} = \ddot{\rho} - \frac{1}{\rho}\left(\dot{r}_{12}^{(y)} + \dot{r}_{12}^{(z)}\right)^2$$

This equation indicates that g_{12}^{LOS} is not equivalent to $\ddot{\rho}$. In addition to $\ddot{\rho}$ term, it also contains a geometric correction term $\left(\dot{r}_{12}^{(y)} + \dot{r}_{12}^{(z)}\right)^2/\rho$. This correction term involves the transverse (y) and radial (z) components of the intersatellite relative velocity $\dot{r}_{12}$

and is therefore analogous to a centrifugal acceleration term. Using the reference dynamic orbit, the residual form can be reduced as:

$$\delta g_{12}^{LOS} = \delta\ddot{\rho} + \Delta_0$$

Here, $\delta\ddot{\rho}$ denotes the KBR/LRI range-acceleration residual, Δ_0 represents the residual associated with the geometric correction term, and δg_{12}^{LOS} is the LGD. Ghobadi-Far et al. (2018) developed an accurate method for estimating δg_{12}^{LOS} by explicitly accounting for Δ_0 as a second-order correction. This method uses the stable admittance relationship between range-acceleration residuals and LGD at frequencies above 5 CPR to convert KBR/LRI residuals into more accurate LGD measurements. Therefore, below 1 mHz, the KBR/LRI range-acceleration residuals may be dominated by geometric or centrifugal acceleration effects, whose spectral power is even higher than that of the range-acceleration residuals within this frequency band, as shown in Figure 1 of Ghobadi-Far et al. (2018).

These geometric effects included in the low-frequency component (<1 mHz) do not represent true hydrological mass change signals and are an important reason for the discrepancy between the KBR/LRI residuals and the low-frequency LGD synthesized from L2 data products. Thus, the low-frequency LGD below 1 mHz is more appropriately provided by L2 products, whereas the high-frequency component above 1 mHz can be extracted from KBR/LRI residuals using the transfer function.

Line 209-213: Beware that now your climatological fit is also influenced by the effect related to the prior mission (GRACE). Did you remove any solutions in this climatological fit? And if yes, which ones and why (not)? Before synthesis/climatological fit, did you perform any form of filtering (i.e. Gaussian, DDK, …)?

R1C21: In this study, the climatology fit is estimated using GRACE CSR RL06 and GRACE-FO CSR RL06.3 gravity field solutions from 2002 to 2023. The processing strategy is as follows. First, we collect the spherical harmonic solutions, replace $C_{2,0}$ and $C_{3,0}$ with SLR-derived estimates, and remove the static field of GOCO06s. Second, for each Stokes coefficient time series, we perform a least-squares fit consisting of a linear trend, a seasonal term, and residuals, and remove outliers based on the fitted residuals. Specifically, months with residuals exceeding three times the standard deviation are excluded. Third, the climatological coefficients for each target date are obtained from the fitted model, and the climatological LGD is then synthesized from these coefficients.

To make this procedure clearer, we have added Figure S6, which shows examples of the climatological fitting for six selected Stokes coefficients. The red curves denote the fitted climatological models, and the vertical black lines indicate the excluded outliers. For any given date, the corresponding climatological gravity-field coefficients are obtained from the fitted curves and then used to synthesize the climatological LGD. We also clarify that no spatial filtering is applied to the Stokes coefficients before the synthesis or climatological fit. This is because computing LGD at satellite altitude from the Stokes coefficients is an upward-continuation process and therefore naturally suppresses short-wavelength noise.

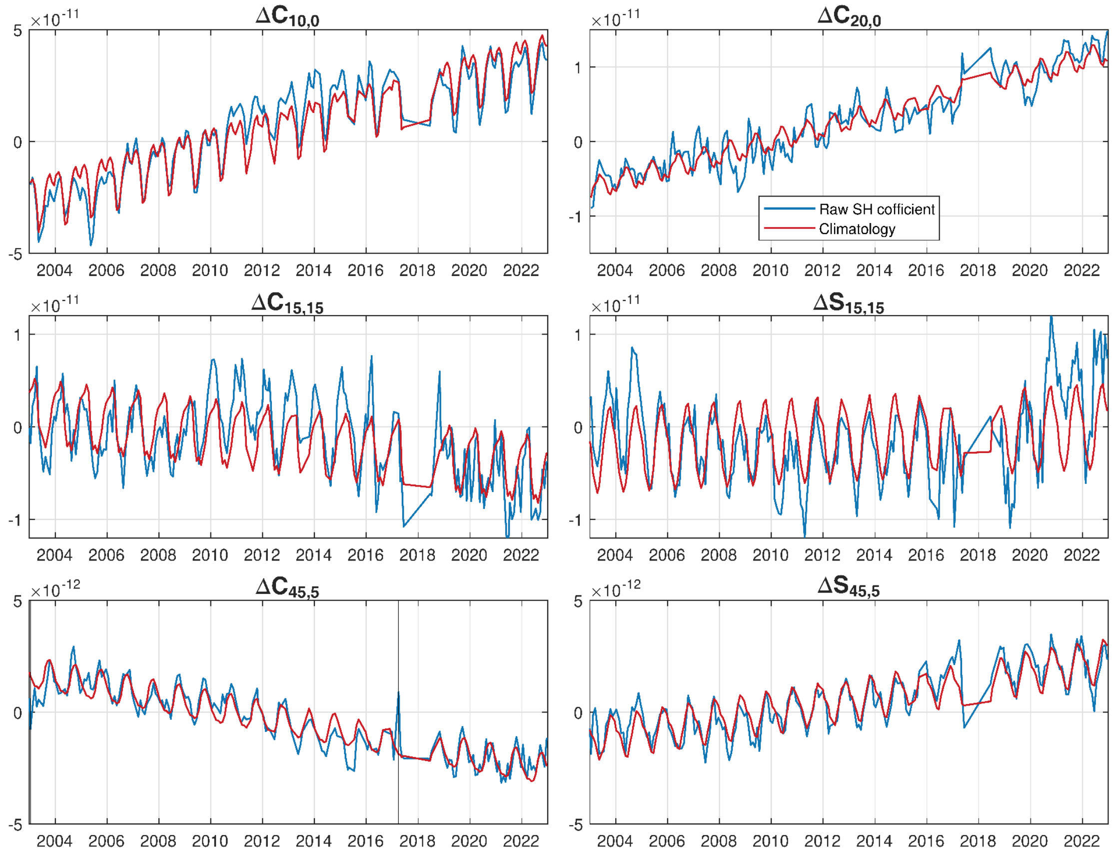

Figure S6. Examples of monthly time-series of GRACE and GRACE-FO L2 gravity field (Stokes') coefficients (blue) and their climatology (red). Vertical black lines mark outliers in the raw spherical harmonic coefficients.

2.4:

What filter was used? What are the variables used for it? This information is missing. You are not showing the signal below 1 mHz, which you mention needs to be replaced by L2. I would this needs to be added for clarity and completeness.

R1C22: We used a 6th-order Butterworth band-pass filter. The input variables are the time series s, the number of samples n_d, the lower and upper cutoff frequencies f_1 and f_2, the sampling interval Δt (5 s for KBR and 2 s for LRI), and the filter order parameter. The filter is applied in a zero-phase-shift manner. We cannot show a physically meaningful spectrum of the LGD measurements below 1 mHz because the transfer function is only applied above 1 mHz.

Line 241: explain what you mean by "a full-spectrum gravity change signal is sought after.". Which degrees are currently being "removed" or filtered. This should be made explicit for data users.

R1C23: Here, "full-spectrum" refers to an LGD signal that includes the low-frequency component below 1 mHz, rather than only the transfer-function-derived component above 1 mHz. This applies to both LGD_full and LGD_band. We have added a schematic figure (Figure S7) to explicitly show the frequency content of the different LGD products. For LGD_full, no signal is removed or filtered. For LGD_band, only the high-frequency part is filtered, namely frequencies above 10 mHz for KBR-LGD and above 20 mHz for LRI-LGD. The low-frequency component below 1 mHz is supplemented with L2-derived LGD.

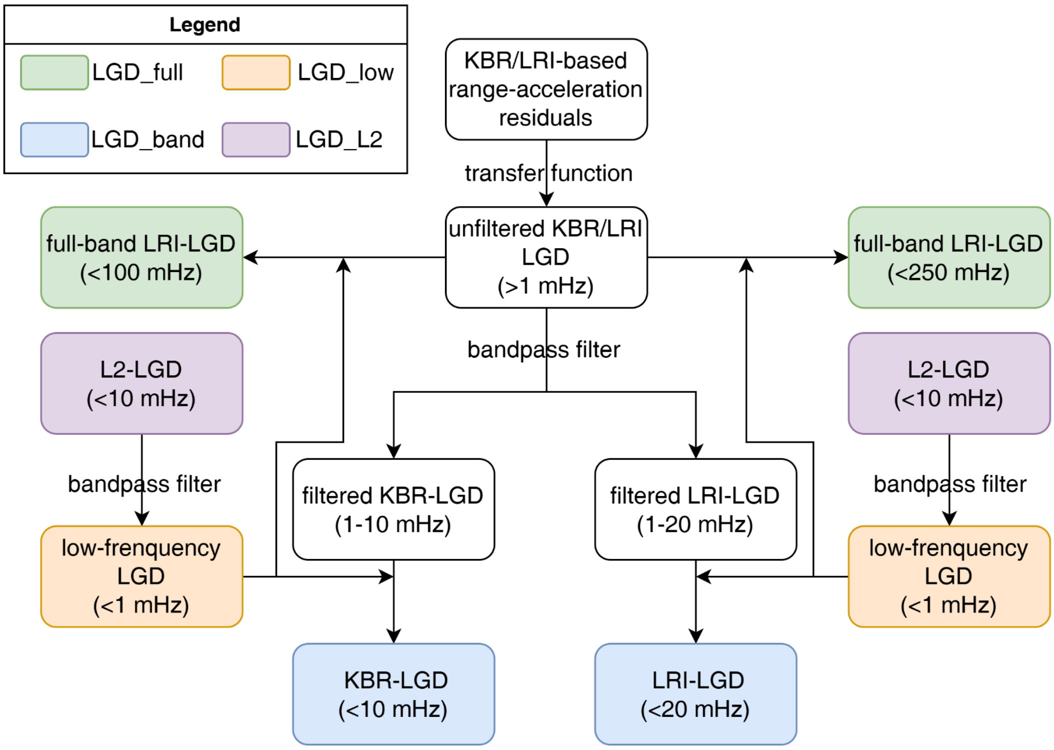

Figure S7. Schematic illustration of the frequency content of the LGD products derived from KBR/LRI observations and Level-2 solutions.

Section 3:

3.1.

1) What is the reasoning for using .txt as a file format? Aren't there more space efficient data formats which would aid in the usage of this dataset?

R1C24: Thank you for this helpful comment. We agree that there are more space-efficient file formats than plain text (e.g., NetCDF). Our main reason for using .txt is accessibility and portability. The dataset is intended for broad use across different communities, and plain-text files can be easily read, inspected, and processed without requiring specialized software or format-specific libraries. This makes the dataset more immediately usable for a wide range of users and computing environments. We will consider providing a more compact format, such as NetCDF, in a future release to improve storage efficiency and facilitate large-scale use of the dataset.

2) How were the mid longitude, latitude and most importantly altitude computed? This is important information because there is a difference between simple altitude mean (i.e. (alt_1+alt_2)/2) and the more geometrically relevant mid altitude due to the orbital

curvature. This needs to be added (especially due to the fact that LGDs are related to altitude).

R1C25: In our processing, the midpoint is not computed as the simple mean of the two individual satellite altitudes. Instead, at each common epoch, we first define the midpoint in the Earth-centered Cartesian frame as the geometric midpoint of the two satellite position vectors,

$$\mathbf{r}_{\text{mid}} = (\mathbf{r}_1 + \mathbf{r}_2)/2$$

The midpoint longitude and latitude are then derived from this vector, and the satellite altitude is obtained from

$$r_{\text{mid}} = \|\mathbf{r}_{\text{mid}}\|$$

i.e., the geocentric radius of the midpoint. The released satellite altitude is equal to r_{mid} minus the radius of the Earth (6378136.3 m).

Note that this midpoint location is mainly introduced to provide a consistent and comparable geographic definition for organizing and visualizing the along-track LGD measurements on a global scale. It should not be interpreted as implying that the LGD strictly represents the gravity signal at that exact midpoint location in a rigorous physical sense. We have clarified this point in the revised manuscript.

3) Please provide a source of any form to explain the lack of days/files for KBR.

R1C26: In principle, the KBR-LGD dataset should contain 2406 daily files from 1 June 2018 to 31 December 2024, whereas our release contains 2260 files, indicating a total of 146 missing days. Among these missing days, 120 correspond to publicly unavailable L1B observation files, as documented in the official GRACE/GRACE-FO monthly record table (https://archive.podaac.earthdata.nasa.gov/podaac-ops-cumulus-docs/gracefo/open/docs/GRACE_GRACE-FO_Months_RL06.csv), which attributes the gaps mainly to instrument issues, calibration campaigns, etc. The remaining 26 days were removed during our quality-control procedure because the kinematic orbit and/or determined reference dynamic orbit did not meet the quality requirements for reliable LGD generation. We have added this explanation and the corresponding reference to the revised manuscript.

3.2.

1) again essential to mention which components of GOCO06s are used here.

R1C27: Please see our response in R1C14 for details.

2) provide rationale why the signal you see is hydrological in nature. Reference? Rationale?

R1C28: The rationale is that the reference dynamic orbit already accounts for all the currently known background gravitational effects, such as tidal and non-tidal contributions, as well as the non-gravitational accelerations measured by the onboard instruments. Therefore, the residuals between the observed KBR/LRI intersatellite ranging measurements and the corresponding range variations simulated from the reference orbit primarily reflect gravity changes that are not induced by these background models. Over land, such unresolved time-variable gravity signals are expected to be dominated mainly by hydrological mass changes.

We acknowledge that these signals may also contain contributions from other unmodeled or mismodeled processes, such as glacial isostatic adjustment (GIA) and earthquakes. However, GIA mainly affects very long-term variations, while earthquake-related signals are infrequent and generally localized in space (e.g., Rodell and Li, 2023). Therefore, for the purpose of this dataset, the LGD derived from range-rate residuals is expected to primarily represent hydrological mass variations. We have clarified this rationale and added the corresponding reference in the revised manuscript.

3) Line 295: what do you mean by climatological average? This is just the evaluation of LGDs from climatological fit of L2 SH solutions. Needs to be rephrased.

R1C29: Thank you for this comment. What we mean is the LGD synthesized from the climatological fit (i.e., the red curves in Figure S6) of the Level-2 spherical harmonic solutions. We have revised the manuscript accordingly and the revised text now reads: "In contrast, the climatological LGD (LGD_clm; orange curve shown in Fig. 5b) represents the LGD synthesized from the climatological fit of the Level-2 spherical harmonic solutions for July 2020."

4) I would highly recommend to provide more descriptions and rationale on what is actually observed and not only mentioned as "Their differences are mostly from the instantaneous gravity changes with respect to the monthly mean gravity as reflected by the L2 solutions." This needs some mention and explanation.

R1C30: Thank you for pointing this out. We have further clarified that KBR-LGD reflects instantaneous along-track gravity variations, whereas LGD_L2 is synthesized from monthly averaged Level-2 gravity fields. Therefore, their differences mainly arise because KBR-LGD captures short-term mass variations occurring within the month, while LGD_L2 represents only the monthly mean and cannot resolve such intra-month fluctuations. For example, over Bangladesh, the discrepancy between L2-LGD and KBR-LGD reaches about 0.5 nm s^{-2}, indicating that the monthly Level-2 solutions would underestimate the actual magnitude of water mass change. These are reflected in the revised manuscript.

5) Line 298: make it more precise. These are extreme events w.r.t the climatological fit but still at monthly resolution.

R1C31: Thank you for this comment. We agree that the climatological reference is derived from a fit to monthly Level-2 solutions. It should be noted, however, that we use a continuous climatological fit, rather than a stepwise monthly reference (the difference between the two is illustrated in Figure S8), to evaluate the reference field at any given date and then synthesize the corresponding climatological LGD along the actual satellite track. For example, for 18 July 2020, we first extract the spherical harmonic coefficients for that date from the climatological fit (Figure S6), then synthesize LGD along the actual satellite track of that day, and finally subtract this climatological LGD from the instantaneous LGD measurements. Because the LGD measurements themselves are instantaneous, the resulting along-track LGD anomaly can still reflect instantaneous departures from the climatological state. We acknowledge that errors in the climatological fit, including those related to monthly sampling and temporal interpolation, may affect the anomaly estimate. We have revised the manuscript accordingly.

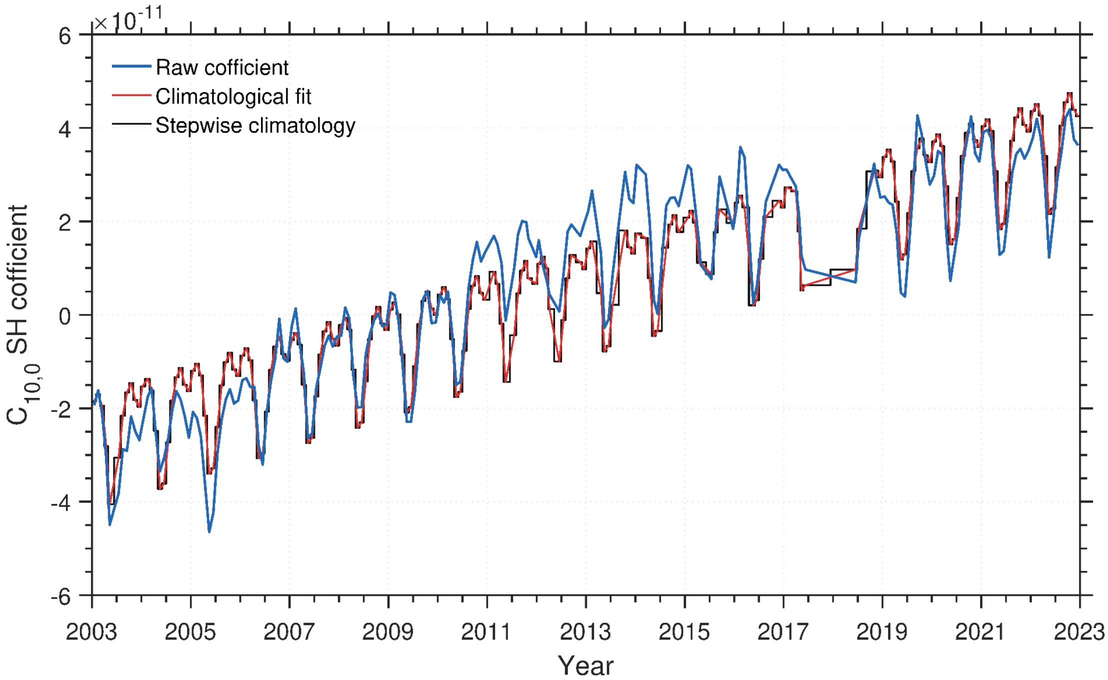

Figure S8. Example of a continuous climatological fit and a stepwise climatology for the $C_{10,0}$ spherical harmonic coefficient.

6) Line 299: "possibly"? This is insufficient. Is this during the monsoon season? Explain.

R1C32: We apologize for the ambiguous wording. In fact, Han et al. (2021) already demonstrated that this rapid increase in water storage, with a change reaching about 17 nm s^{-2} from the event onset to the peak, was caused by Cyclone Amphan during the monsoon season. We have therefore removed the word "possibly" and revised the manuscript accordingly.

7) Line 305-307: provide a reference for the LRI comment.

R1C33: We have revised the manuscript to clarify that the high-frequency oscillations between 30° S and 60° S may be related either to LRI instrument noise or to errors in the AOD background model, and we have added the corresponding references (Ghobadi-Far et al., 2020; Shihora et al., 2022).

8) Line 308: “ultra-long”? I would rephrase to simply long-wavelength signals (about below degree/order 5).

R1C34: Thank you for this comment. We have rephrased it to “long-wavelength.”

9) Line 309: please quantify what this fraction is?

R1C35: We have now quantified this fraction using the variance contribution of the low-frequency component LGD_{low} relative to the band-passed signal LGD_{band}, i.e.,

$$P_{\text{var}} = \frac{\sum_{i=1}^{N}(LGD_{low,i} - \overline{LGD_{low}})^2}{\sum_{i=1}^{N}(LGD_{band,i} - \overline{LGD_{band}})^2} \times 100\%$$

where $LGD_{low,i}$ and $LGD_{band,i}$ denote the low-frequency LGD and bandpass LGD at the i-th sample, respectively, $\overline{LGD_{low}}$ and $\overline{LGD_{band}}$ are the corresponding mean values, and N is the total number of samples shown in Figure 5 (in main text). Based on this definition, the variance contribution of LGD_{low} to LGD_{band} is about 7%. We have added this quantitative description to the revised manuscript.

10) I highly recommend the use of quantification of signal power (i.e. RMS) to be able to better understand the “power” of the different types of LGD signals.

R1C36: Thank you for this helpful suggestion. We do not consider the RMS of a short example arc to be the most appropriate metric for comparing these signals, because their power is more meaningfully characterized in the frequency domain. Nevertheless, to provide a quantitative indication of their relative importance, we evaluated the variance contribution as described above (see the equation in R1C35). Based on this calculation, LGD_{band} accounts for about 98% of the variance of LGD_{full}.

3.3.

1) Line 311-315: I recommend providing the difference plot to see/verify/validate that these signals are as they should be.

R1C37: Thank you for this suggestion. However, a point-by-point difference plot between KBR-LGD and LRI-LGD cannot be provided, because their along-track sampling is not identical: the KBR sampling interval is 5 s, whereas the LRI sampling interval is 2 s. Instead, we directly show the LRI–KBR signal in the 10–20 mHz band, which captures the main part of the difference between the two datasets. This is because the LGD derived from the two sensors is nearly identical in the 1–10 mHz band (see Figure 3 in the main text), and therefore, to a large extent, their differences mainly arise from the 10–20 mHz range. As shown in Figure S9, the most significant signals appear over Greenland, Antarctica, and Alaska, which is consistent with the findings of Peidou et al. (2022). At the global scale, the RMS of the LRI-LGD within the 10–20 mHz is 0.25 nm/s^2. We have added this explanation to the revised manuscript.

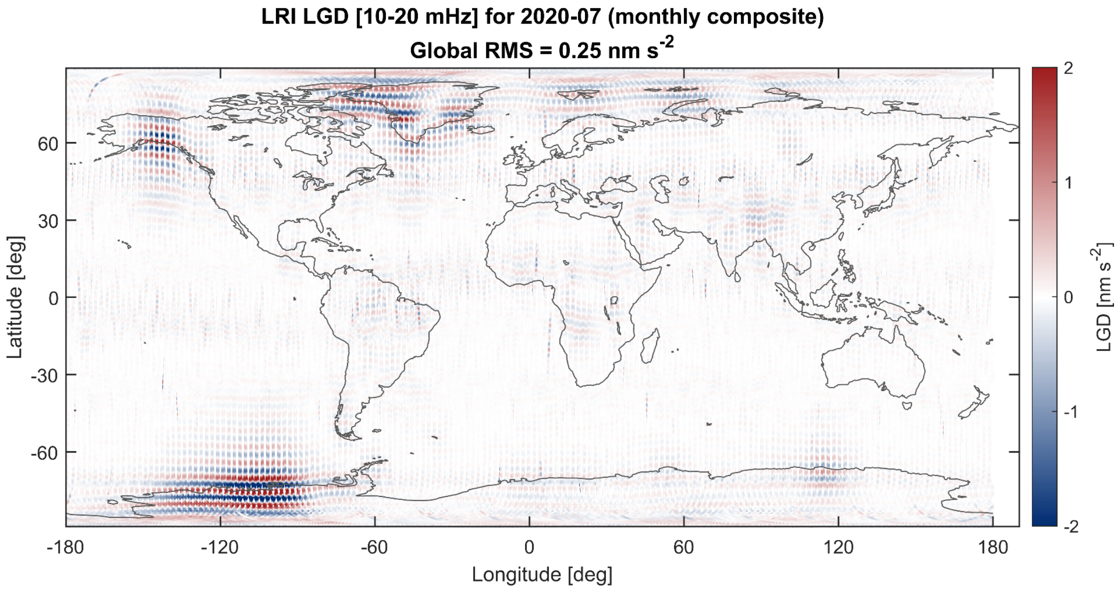

Figure S9. Global distribution of monthly composite LRI-LGD in the 10–20 mHz band for July 2020.

2) Please make the colorbar and its label bigger.

R1C38: Done.

3.3.

1) Figure 8: increase the size of the colorbar and its label.

R1C39: Done.

2) Lines 370-375: I do not follow what/why you are Gaussian filtering the time series. Please rephrase and improve for readability.

R1C40: When constructing a regional LGD time series, we need to integrate the along-track LGD measurement time series crossing the study area, which is done through a weighted average (as shown in Figures S10a and S10b). Sensitivity analysis (Figures S10c and S10d) shows that the maximum LGD response is contributed by surface mass directly beneath the satellite track, and the response decays rapidly with increasing distance from the load center. Therefore, when focusing on a specific study region, LGD observations near the boundary are more likely to be influenced by mass changes outside the target region and should not be integrated with equal weight. For this reason, we apply a Gaussian-based weighting when integrating the along-track LGD observations into a regional time series. The corresponding weighting formula is:

$$LGD_i = \frac{\sum_{j=1}^{N} w_j LGD_{i,j}}{\sum_{j=1}^{N} w_j}$$

where $LGD_{i,j}$ is the j-th along-track LGD measurement on date i. For a given date i, LGD_i represents the regional LGD (Figure S10b) derived from the LGD measurements crossing the target region. Here, N is the number of observations within the target region, and w_j is the Gaussian weight assigned to the j-th observation, as illustrated by the blue curve in Figure S10d. It should be noted that this is not the only possible weighting or integration strategy for deriving regional variations; other schemes may also be used, depending on the user's purpose. We have revised the manuscript to make this point clearer and to improve readability.

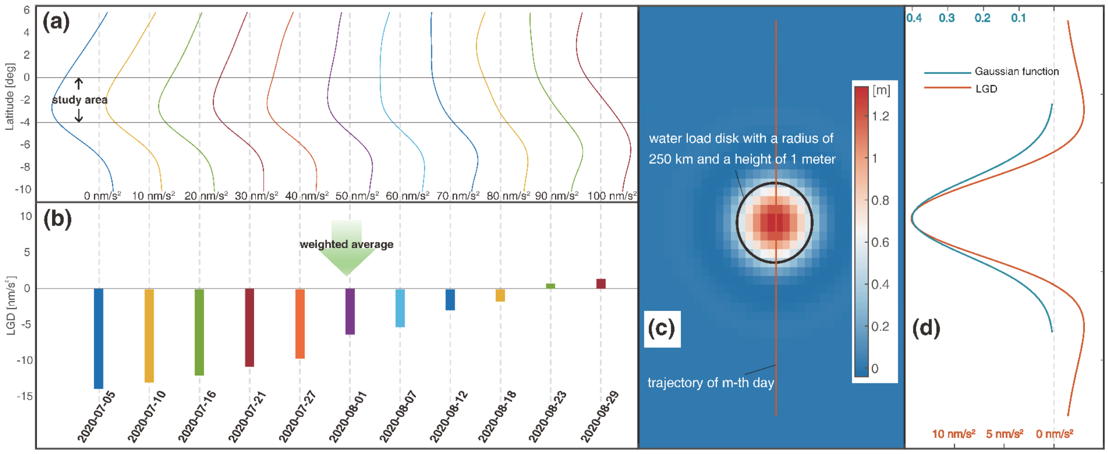

Figure S10. Schematic illustration of the Gaussian-weighted construction of the regional LGD time series. (a) Along-track LGD profiles crossing the target study area on different dates. (b) Regional LGD results obtained from the Gaussian-weighted averaging of the along-track observations within the target area. (c) Example of the modeled LGD response to a water load and the satellite ground track used for the sensitivity analysis. (d) Gaussian weighting function and the corresponding along-track LGD response used to illustrate the weighting strategy.

Section 4:
4.2. Very interesting methodology of standardisation.

R1C41: We appreciate the reviewer's recognition of our standardization methodology.

1) Line 477:" evident short-term wiggles" rephrase and provide quantification.

R1C42: Thank you for this comment. We have revised the manuscript to describe these features more precisely as short-term fluctuations. Because the overall LGD amplitude in Eastern Australia is relatively small, we quantify these fluctuations using a relative measure rather than an absolute RMS value, i.e.,

$$R = \frac{\mathrm{RMS}(LGD_{KBR} - LGD_{L2})}{\mathrm{RMS}(LGD_{KBR})} \times 100\%$$

Using this metric, Eastern Australia shows the largest relative level of short-term fluctuations among the five regions, reaching 46%, compared with 23% for the Mississippi, 14% for the Amazon, 15% for South Sudan, and 19% for Bangladesh. We have revised the manuscript accordingly.

2) Line up to 481: you did not see the effects of the so-called lobes of the LGD observable. Lobes also make the localization of geophysical signals in small regions much more complicated.

R1C43: We agree that the lobes of the LGD observable complicate the localization of geophysical signals in small regions. To examine this issue more explicitly, we performed additional sensitivity experiments using idealized water loads of different scales and positions relative to the target area. The results are shown in Figure S11.

These experiments indicate that the influence of external mass changes on the regional LGD is not controlled by side lobes alone, but more generally by signal leakage associated with the spatial response of the LGD observable. In practice, this leakage depends mainly on the magnitude and distance of the external load relative to the study area. For example, in Figure S11b, the contribution from the nearby external load is dominated by the main lobe rather than by the side lobes. In Figure S11c, where the load is located farther away, the side-lobe contribution becomes visible; however, its magnitude is much smaller than that associated with the main-lobe response. The same behavior is also evident for the 400 km load experiments (Figure S11d–e) but, in this case, the main-lobe contribution becomes more pronounced as the load radius is larger (400 km). This is because the LGD response decays rapidly away from the load center.

Therefore, we agree that the LGD signal cannot be interpreted as being strictly localized within the study region. Instead, it should be regarded as being primarily sensitive to mass variations within and near the target area, while also being affected by leakage from surrounding areas. As discussed in our response above (see R1C40), the Gaussian weighting adopted in our study can mitigate this influence to some extent, although it cannot remove it completely. We have clarified this point in the revised manuscript.

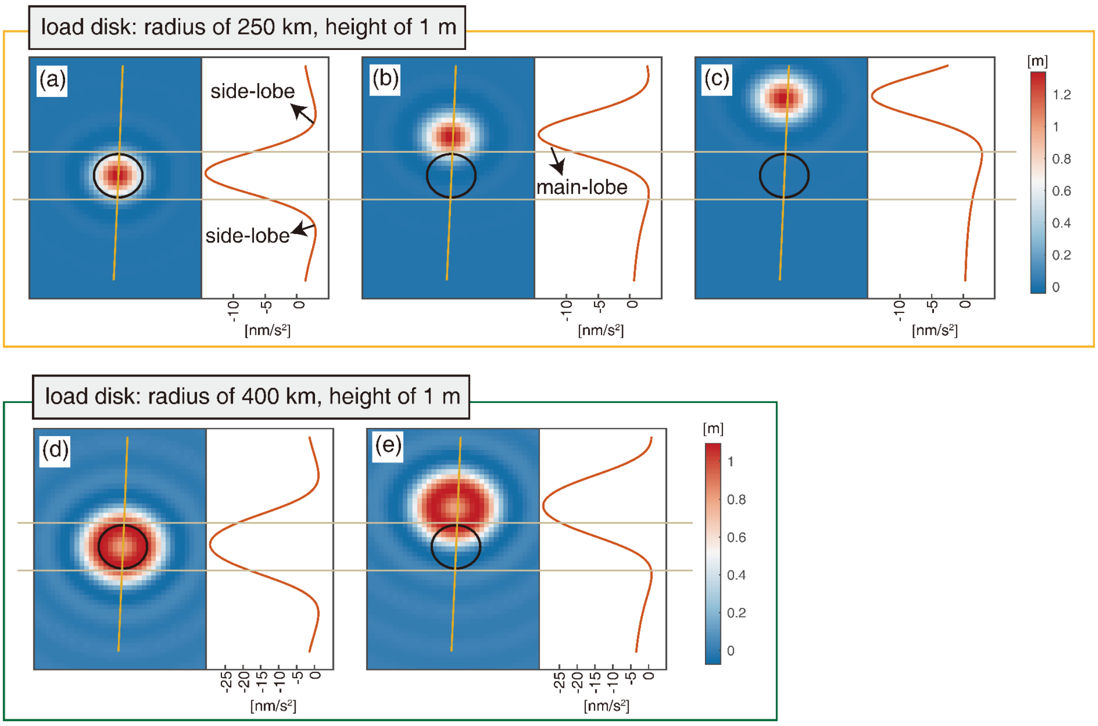

Figure S11. Sensitivity experiments illustrating leakage into a target study region from external water loads of different magnitudes and positions. Panels (a)–(c) show the responses to a 1 m water load with a radius of 250 km, while panels (d)–(e) show the corresponding responses for a 1 m high water load with a radius of 400 km. In each panel, the left map shows the imposed water load (red shading), the target study area (black circle), and the satellite ground track (yellow line), whereas the right curve shows the corresponding along-track LGD response.

3) Line 488: it is unclear what you mean by "sub-monthly" dynamics when mentioning the L2 based solutions. These are monthly by definition.

R1C44: We apologize for the ambiguity. We have revised the manuscript accordingly, and the revised text now reads: "It is important to note that L2-LGD is synthesized from monthly Level-2 gravity fields and therefore represents only the monthly mean state, rather than true sub-monthly variability."

4) I would highly recommend adding these indices as supplement datasets.

R1C45: It is difficult to provide a universal MCI dataset directly, because the calculation of MCI first requires the definition and localization of the target study area, which depends strongly on the user's specific purpose and application. In this sense, MCI is not a fully generic product like the along-track LGD itself. As an alternative, we provide the open-source code for generating the index, so that users can flexibly compute MCI for their own regions and objectives. The code is available at https://github.com/mTangcute/Mass-Change-Index.

Section 5:
5.1.
1) I would recommend of adding these difference in ocean tidal models as there are significant in frequency domain.

R1C46: Following the reviewer's recommendation, we have now examined the spectra of the LGD differences resulting from two alternative ocean tide models (FES2014b and GOT4.7), focusing on the main tidal constituents K1, M2, O1, and S2. The results show that the amplitudes of model differences remain much smaller than the LGD signal itself. In terms of RMS, the values are 0.14, 0.17, 0.08, and 0.10 nm/s^{-2} for K1, M2, O1, and S2, respectively. By comparison, the RMS of the LGD signal in the corresponding signal bands is 5.00 nm/s^{-2} for KBR and 5.01 nm/s^{-2} for LRI. We have added this discussion and the corresponding figure to the revised manuscript.

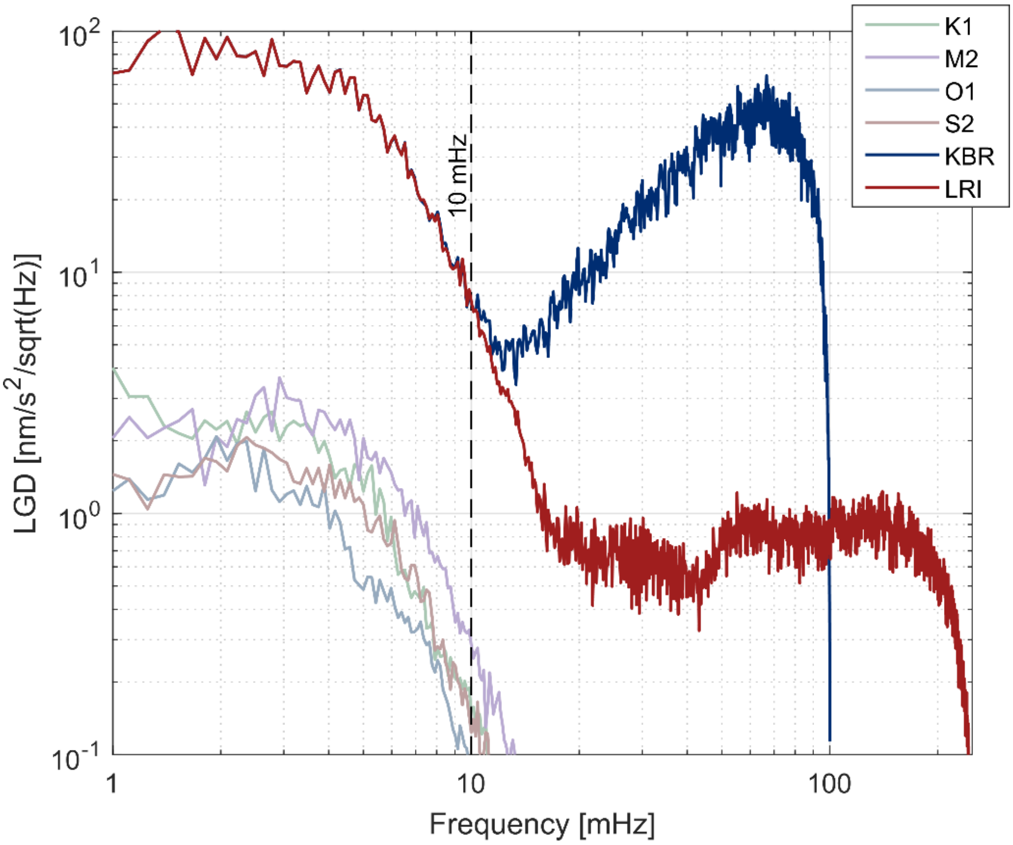

Figure S12. Amplitude spectral density of the LGD differences on 18 July 2020 resulting from two alternative ocean tide models (FES2014b and GOT4.7), shown for the main tidal constituents K1, M2, O1, and S2. The KBR-LGD and LRI-LGD spectra are also shown for comparison.

2) Explain still the benefits of using GOCO06s either way if you either way remove frequencies above 10 mHz for the more "reliable" KBR version.

R1C47: The benefit of using GOCO06s is not limited to the frequency range above 10 mHz. First, the improved high-frequency accuracy of GOCO06s helps reduce errors in the reference dynamic orbit during orbit determination, which in turn can also reduce the leakage of modeling errors into lower frequencies. Second, GOCO06s has indeed been shown to perform better in the 17–35 mHz band for LRI-LGD (see Fig. 1 of Ghobadi-Far et al., 2020). Therefore, although frequencies above 10 mHz are not retained in the final KBR-based product, the use of GOCO06s still improves the intermediate orbit determination and residual generation steps, and is thus beneficial to the overall processing. For these reasons, we finally adopted the widely used and well-validated GOCO06s model.

3) The noise models you are providing are not very accurate and do not follow the noise-dominated section of the spectrum. This must be revised. The simple noise models are clearly not appropriated. There are other "better" analytical models. Please provide the low-frequency noise models too.

R1C48: The noise models used in the original manuscript were intended to represent the currently recognized nominal sensor noise levels of KBR and LRI. However, we acknowledge that these nominal models do not adequately follow the noise-dominated sections of the observed spectra. Therefore, in the revised manuscript, we have added empirical fits (see light blue and light red curves in Figure S13) to the noise-dominated parts of the observed spectra using a power-law model, i.e.,

$$ASD_{KBR-LGD}(f) = 3332\, f^{1.5006}\ (f > 10\ \text{mHz})$$

$$ASD_{LRI-LGD}(f) = 1.2\, f^{0.1687}(f > 20\ \text{mHz})$$

where f is the frequency in Hz. We do not provide the low-frequency noise model, because the low-frequency part of the spectrum is not dominated by sensor noise alone, but to a large extent, by other sources such as background-model errors.

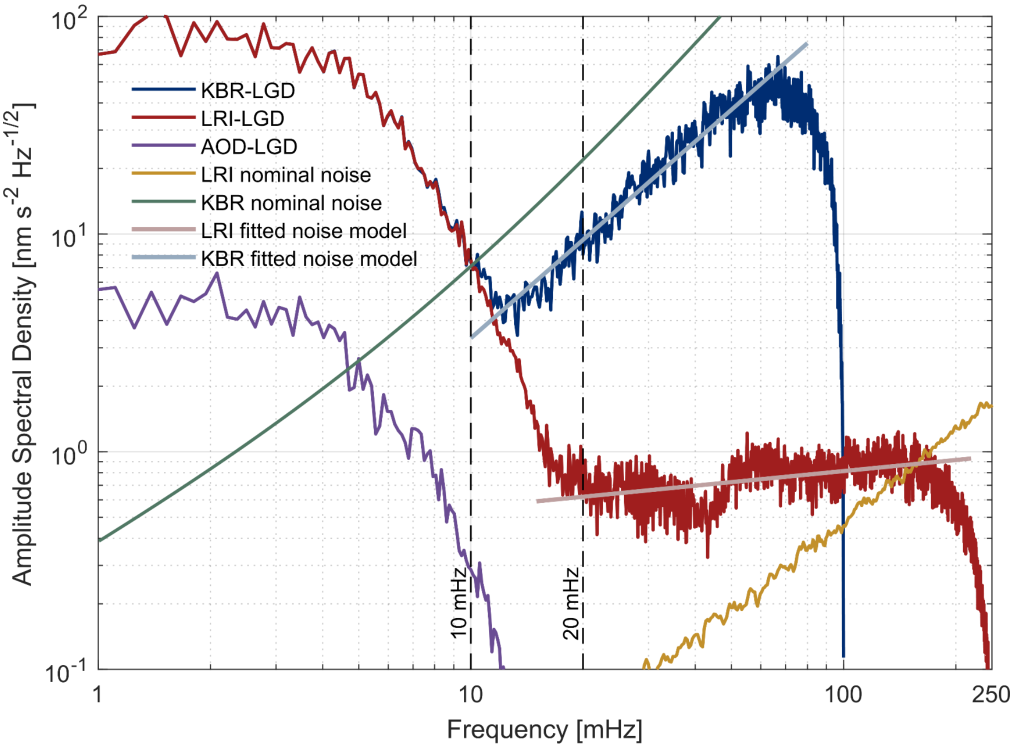

Figure S13. Amplitude spectral densities of KBR-LGD, LRI-LGD, and AOD-LGD observations. The fitted noise models for KBR and LRI are shown as light blue and light red lines, respectively, together with the nominal instrument noise levels (yellow and green curves).

4) Given all of these findings, I would provide these results in a summarizing table with a certain “prediction” of total uncertainty. Without the latter it is very difficult to understand what the uncertainty is.

R1C49: Thank you for this helpful comment. Note that a rigorous uncertainty estimate for LGD is difficult to provide because LGD is an along-track observable with frequency-dependent and spatially variable sensitivity. Its error budget is controlled not only by sensor noise but also by background-model and processing-chain uncertainties, which together make the problem inherently complex. In practice, the uncertainty assessment is more appropriately carried out in the spectral domain. Here, we add a summary table that compiles the main error sources and their magnitudes in the relevant frequency bands (Table S1).

The high-frequency instrumental noise has already been largely suppressed by filtering; therefore, in the used signal bands (<10 mHz for KBR-LGD and <20 mHz for LRI-LGD), the remaining uncertainty is mainly dominated by background-model errors. However, we cannot quantify the true modeling errors of these background models, which would be required for their direct propagation into LGD uncertainty. Instead, we use the differences between alternative models (e.g., different versions of AOD model) as a practical lower-bound estimate of their impact on LGD.

Table S1. Summary of the main error sources affecting LGD and their estimated magnitudes, with 18 July 2020 shown as an example

Error source	description
KBR sensor	RMS = 5.0 nm/s^2 in the 1–10 mHz band; RMS = 9.5 nm/s^2 in the 10–100 mHz band
LRI sensor	RMS = 5.0 nm/s^2 in the 1–20 mHz band; RMS = 0.4 nm/s^2 in the 20–250 mHz band
Difference between ocean tidal models (FES2014b vs. GOT4.7)	RMS = 0.2 nm/s^2 in the 1–10 mHz band, which is about one order of magnitude smaller than the LGD signal
Difference between AOD models (RL07 vs. RL06)	RMS = 0.3 nm/s^2 in the 1–10 mHz band, which is about one order of magnitude smaller than the LGD signal

5.2.

1) Here it is essential to mention (highly incomplete): a. What is the EWH derived from? Which solution? This needs to be made explicit as a must. b. Which post-processing steps were made to result in these EWH time-series? (i.e. filtering? …) c. Which LGD is used here? The full band LGD? This needs to be made explicit. d. Make explicit by RMS or any other measure than R^2 what the errors of the relationships estimated are.

R1C50: We have clarified that the EWH is derived from the CSR RL06.3 spherical harmonic solutions. In addition to the data products, the preprocessing steps are also consistent with those used for the L2-LGD synthesis, including replacement of the degree-2 and degree-3 zonal coefficients, removal of the GOCO06s static field, and truncation to degree and order 60. In addition, decorrelation and Gaussian smoothing with a 350 km radius (Swenson and Wahr, 2006) are applied in the spherical harmonic synthesis to derive the EWH. The LGD used here is the band-passed product, i.e., LGD_band. Following the reviewer's suggestion, we have also used the RMSE of the regression residuals to quantify the uncertainty of the estimated relationship more explicitly. The resulting RMSE values are 46.8 mm for the Amazon, 24.4 mm for Bangladesh, and 26.1 mm for South Sudan. We have added this information to the revised manuscript.

2) What solution do you propose to correct for such effects? These seem to be quite significant (i.e. LGDs at 450 km are not similar to 550 km).

R1C51: A key approach is to reduce all observations to a common observation geometry. For regional applications, such as the 4° × 4° box defined in our study, we propose to reduce the LGD measurements to a common reference orbital altitude and a common crossing longitude relative to the study-area center. In practice, this can be done using scale factors derived from the fitted sensitivity curves obtained in our analysis (Figure S14c and S14f). These scale factors can be used to account for the dependence of LGD amplitude on orbital altitude and on the offset between the satellite track and the center of the target region. Another possible solution is to invert all LGD observations into equivalent surface mass changes. In that case, the observations are converted into an Earth surface-related quantity, which would make measurements acquired under different orbital geometries more comparable. We have added this discussion to the revised manuscript.

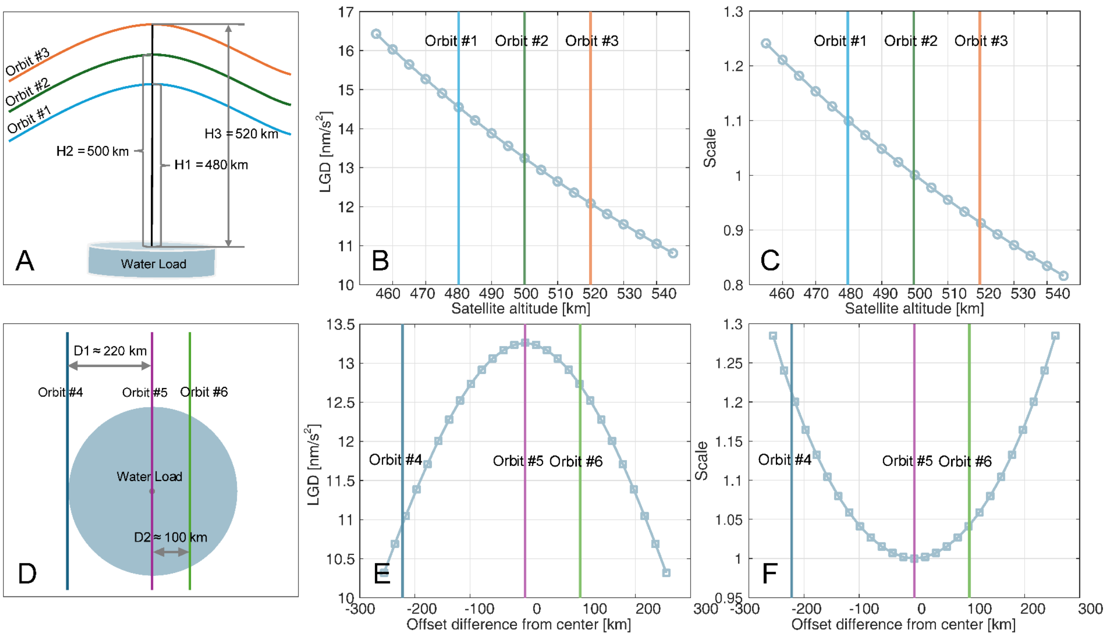

Figure S14. Influence of satellite altitude and track offset on LGD measurements. (a) Schematic illustration of different orbital altitudes over the same water load. (b) Simulated LGD amplitude as a function of satellite altitude. (c) Corresponding scale factor for reducing LGD to a common reference altitude (i.e., 500 km). (d) Schematic illustration of different track offsets relative to the load center. (e) Simulated LGD amplitude as a function of offset from the load center. (f) Corresponding scale factor for reducing LGD to a common reference offset (0 km).

3) What other orbital effects do you believe could affect the LGDs. Explain why did you limit yourself to these two.

R1C52: We focused on these two factors because the LGD response to the same surface mass load can differ substantially between different satellite trajectories. The dominant causes of this difference are the orbital altitude at which the satellite crosses the study region and the longitudinal offset between the track and the load center. Another possible orbital effect is whether the region is crossed during an ascending or a descending pass. Previous studies (e.g., Han et al., 2021) have shown that the difference between ascending- and descending-track LGD responses is relatively small. When only one track direction (ascending or descending) is used consistently, this effect can be neglected to first order. It should also be noted that the lobes discussed above (see R1C43) should be regarded as a geometric characteristic of the LGD sensitivity kernel, rather than as an orbital effect. We have clarified this point in the revised manuscript.

Conclusion:
1) Provide more explanations on uncertainty, this is an essential component of your dataset.

R1C53: Please see our response in R1C49 for details. We have added a dedicated explanation of uncertainty in the revised manuscript.

2) Similar for LGD-EWH relations. Make sure you explain what solution was used here.

R1C54: Please see our response in R1C50 for details. We have clarified the information in the revised manuscript.

3) Again not sure about this "climatological mean".

R1C55: Here, "climatological mean" refers to the climatological LGD. A more detailed explanation is provided in our responses in R1C21 and R1C31.

4) Another essential aspect related to altitude and offset effects needs to be added for completeness.

R1C56: In the revised manuscript, we have now clarified that these two factors not only affect the LGD amplitude itself, but also influence the comparability of observations acquired from different satellite tracks. We have therefore added a discussion on how LGD measurements may be reduced to a common observation geometry when regional comparisons are needed. Please see our response to Comment R1C51 for the detailed explanation.

Response to Reviewer #2's comments

GENERAL:

The authors propose to recover surface water mass change from laser measurements data provided by the GRACE-FO mission and reduced for continental hydrology. This type of data ensures a better temporal resolution that enables to detect intra-month mass variations due to climatic events more accurately. Mapping of surface water mass is fast by considering the transfer function approach developed previously by Ghobadi-Far et al. (2018). The following discussion about the data frequency content and its exploitable bandwidth of the KBR and Laser Ranging Interferometry (LRI) related to surface spatial resolution remains very interesting, even if the question of improving the spatial resolution itself is much debatable due to remaining cross-track errors by considering the Ghobadi-Far et al. filtering, as it is shown numerically in the document. Moreover, the availability of these new type of LRI dataset is proposed and this would be really appreciated by research community. The quality of the presentation of this original work is very good and deserves to be published in ESSD once some minor corrections will be made (see my comments below).

R2C1: We sincerely thank Dr. Ramillien for reviewing this work. We appreciate the reviewer's comment regarding the interpretation of spatial resolution. In fact, our aim is to provide a dataset with emphasis on temporal resolution, rather than spatial resolution, for prompt detection of short-term mass change. To avoid any possible misunderstanding, we have carefully revised the manuscript to clarify this point where appropriate.

MINOR CORRECTIONS

P.5. It would be simpler to explain that the raw along-track LRI observations are reduced in the GOCO6s software from known accelerations, including gravitational potential models listed in Table 1.

R2C2: Thank you for this helpful suggestion. We now explicitly state that the first step aims to reduce the raw along-track observations (LRI1B and KBR1B) by removing all known gravitational and non-gravitational contributions unrelated to terrestrial hydrological mass variations.

P.8. "using least-squares": is this a kind of 6-parameter least-square adjustment for each SH coefficient (constant term + linear trend + annual and semi-annual terms)? Please precise.

R2C3: We clarified. The least-squares adjustment used here is not a six-parameter model. Instead, each cosine and sine spherical harmonic coefficient is fitted separately using a 13-parameter model comprising one linear trend and 12 monthly climatological coefficients, one for each calendar month. The model can be expressed as:

$$y(t_i) = \dot{y}(t_i - t_0) + \sum_{k=1}^{12} M_k(t_i)\beta_k + \varepsilon_i$$

where $\dot{y}$ denotes the linear trend, t_0 is the reference epoch of GOCO06s (i.e., 2010.0), $M_k(t_i)$ is a monthly indicator function, and β_k is the climatological coefficient for month k. An initial fit is performed, observations with residuals exceeding three standard deviations are identified as outliers, and the model is then refitted after excluding these observations. We have added appropriate details to the revised manuscript. This explains the climatological patterns better than a combination of the sinusoidal (annual + semi-annual) functions.

P.16. "20° of the equators": do you mean a 40° band of latitude centered on the Equator? Please precise.

R2C4: Yes. We have revised the wording to "within ±20° of the Equator" to make it more precise.

P.20. "southeastern United States (SEUS)": "SouthEastern United States (SEUS)".

R2C5: Done.

In all the document:
Please check the definition of acronyms, e.g. SEUS looks to be used in the text before being defined. Write "Line-O-Sight (LOS)" instaed of "line-of-sight (LOS)"

R2C6: Thank you for these careful suggestions. We have thoroughly reviewed the manuscript to ensure that all acronyms (e.g., Southeastern United States) are defined at their first occurrence. In addition, we have revised line-of-sight (LOS) to Line-of-Sight (LOS) and ensured consistent usage throughout the manuscript.

Text in the figures are sometimes too small, e.g. Figures 7 and 9. Please redraw them with larger text if necessary.

R2C7: Revised. We have enlarged the text size in Figures 7 and 9 to improve readability.

References

Ghobadi-Far, K., Han, S. C., Allgeyer, S., Tregoning, P., Sauber, J., Behzadpour, S., Mayer-Gürr, T., Sneeuw, N., and Okal, E.: GRACE gravitational measurements of tsunamis after the 2004, 2010, and 2011 great earthquakes, J. Geod., 94, https://doi.org/10.1007/s00190-020-01395-3, 2020.

Ghobadi-Far, K., Han, S. C., Weller, S., Loomis, B. D., Luthcke, S. B., Mayer-Gürr, T., and Behzadpour, S.: A transfer function between line-of-sight gravity difference and GRACE intersatellite ranging data and an application to hydrological surface mass variation, J. Geophys. Res.: Solid Earth, 123, 9186–9201, https://doi.org/10.1029/2018JB016161, 2018.

Han, S. C., Ghobadi-Far, K., Yeo, I. Y., McCullough, C. M., Lee, E., and Sauber, J.: GRACE Follow-On revealed Bangladesh was flooded early in the 2020 monsoon season due to premature soil saturation, Proc Natl Acad Sci U S A, 118, https://doi.org/10.1073/pnas.2109086118, 2021a.

Peidou, A., Landerer, F., Wiese, D., Ellmer, M., Fahnestock, E., McCullough, C., Spero, R., and Yuan, D. N.: Spatiotemporal Characterization of Geophysical Signal Detection Capabilities of GRACE-FO, Geophys. Res. Lett., 49, https://doi.org/10.1029/2021gl095157, 2022.

Rodell, M. and Li, B.: Changing intensity of hydroclimatic extreme events revealed by GRACE and GRACE-FO, Nat. Water, 1, 241–248, https://doi.org/10.1038/s44221-023-00040-5, 2023.

Shihora, L., Balidakis, K., Dill, R., Dahle, C., Ghobadi-Far, K., Bonin, J., and Dobslaw, H.: Non-Tidal Background Modeling for Satellite Gravimetry Based on Operational ECWMF and ERA5 Reanalysis Data: AOD1B RL07, J. Geophys. Res.: Solid Earth, 127, https://doi.org/10.1029/2022jb024360, 2022.

Swenson, S. and Wahr, J.: Post-processing removal of correlated errors in GRACE data, Geophys. Res. Lett., 33, L08402, https://doi.org/10.1029/2005GL025285, 2006.